SCIENCE CHINA
Information Sciences

A low-complexity ECG processing algorithm based on the Haar wavelet transform for portable health-care devices

Peng LI, Ming LIU, Xu ZHANG and HongDa CHEN

Citation: SCIENCE CHINA Information Sciences **57**, 122303 (2014); doi: 10.1007/s11432-014-5199-0

View online: https://engine.scichina.com/doi/10.1007/s11432-014-5199-0

View Table of Contents: https://engine.scichina.com/publisher/scp/journal/SCIS/57/12

Published by the Science China Press

SCIENCE CHINA
Information Sciences

• RESEARCH PAPER •

December 2014, Vol. 57 122303:1–122303:14
doi: 10.1007/s11432-014-5199-0

A low-complexity ECG processing algorithm based on the Haar wavelet transform for portable health-care devices

LI Peng, LIU Ming*, ZHANG Xu* & CHEN HongDa

State Key Laboratory on Integrated Optoelectronic, Institute of Semiconductors, Chinese Academy of Science, Beijing 100083, *China*

Received July 3, 2014; accepted September 16, 2014; published online October 29, 2014

Abstract This paper presents a simple Electrocardiogram (ECG) processing algorithm for portable health-care devices. This algorithm consists of the Haar wavelet transform (HWT), the modulus maxima pair detection (MMPD) and the peak position modification (PPM). To lessen the computational complexity, a novel no multiplier structure is introduced to implement HWT. In the MMPD, the HWT coefficient at scale 2^4 is processed to find candidate peak positions of ECG. The PPM is designed to correct the time shift in digital process and accurately determine the location of peaks. Some new methods are proposed to improve anti-jamming performance in MMPD and PPM. Evaluated by the MIT-BIH arrhythmia database, the sensitivity (Se) of QRS detection is 99.53% and the positive prediction (Pr) of QRS detection is 99.70%. The QT database is chosen to fully validate this algorithm in complete delineation of ECG waveform. The mean μ and standard deviation σ between test results and annotations are calculated. Most of σ satisfies the CSE limits which indicates that the results are stable and reliable. A detailed and rigorous computational complexity analysis is presented in this paper. The number of arithmetic operations in N input samples is chosen as the criterion of complexity. Without any multiplication operations, the number of addition operations is only about $16.33N$. This algorithm achieves high detection accuracy and the lower computational complexity.

Keywords Haar wavelet transform (HWT), modulus maxima pair detection (MMPD), peak position modification (PPM), ECG processing, low complexity, portable health-care devices

Citation Li P, Liu M, Zhang X, et al. A low-complexity ECG processing algorithm based on the Haar wavelet transform for portable health-care devices. Sci China Inf Sci, 2014, 57: 122303(14), doi: 10.1007/s11432-014-5199-0

1 Introduction

Aged population is a common phenomenon all over the world in the 21st century. It will lead to the incidence of age-related diseases growing rapidly such as the hypertension, the heart disease and the diabetes. Therefore, the physiological signals acquisition [1–4] and processing [5–7] are of great interest to scientists and clinicians. The ECG signals processing has developed rapidly, due to the sudden and high mortality rates of heart diseases. Every patient cannot afford to go to the hospital for the regular check-up. It is limited by the unavailability of proper medical facilities and the growing cost of regular physical examination.

* Corresponding author (email: liuming@semi.ac.cn, zhangxu@semi.ac.cn)

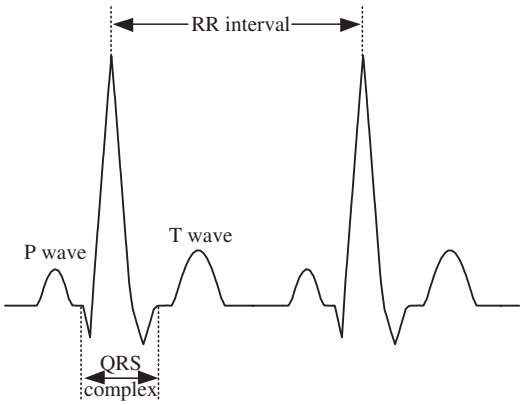

Figure 1 The ECG signals.

This problem can be solved by portable health devices which are widely available and easily affordable by the general public. With the increase of interest in health care, the demand for portable ECG continuous monitoring devices is growing rapidly. Reliable ECG signals can be obtained by devices that have low power consumption and high detection accuracy. Reducing the computational complexity is a good method to lower power consumption. To increase the detection accuracy, the characteristics of ECG signals must be understood at first.

ECG can be characterized as a periodic occurrence of patterns including the P wave, QRS complex (group of Q, R and S waves) and T wave as shown in Figure 1. Compared with the P and T wave, the QRS complex has higher amplitude and provides more information about the heart condition [8]. The heart rate variability (HRV) can be calculated accurately by the interval between R peaks [9]. However, it's particularly difficult to acquire ideal ECG signal. Due to the features of low frequency and weak amplitude, ECG signals are disturbed by different kinds of noises, including the baseline drift, power line interference and motion artifacts [10]. In this sense, avoiding or overcoming these interferences and getting the ideal ECG signals are the most important goals.

There are many classical ECG signal processing algorithms. Based on the slope or amplitude of ECG signals, the time domain algorithm can analyze signals with the least complexity. A typical work is the quad level vector (QLV) algorithm [11], which can compress and classify the ECG signals efficiently. However, the anti-jamming of these algorithms is rather poor and preprocessing like filtering must be done before processing, which would increase the calculation amount of system. Among the frequency domain processing algorithms, the wavelet transform (WT) is one of the most popular methods. In [12], the algorithm can detect three kinds of ECG waveform successfully without any preprocessing, but the work is done on multi-scale transform that increases the computational complexity. As described in [13], the multi-scale mathematical morphology (3M) algorithm can suppress noises and enhance the ECG signals effectively. To achieve these goals, the multi-scale mathematical morphology filtering and the multi-frame differential modulus accumulation are used in this method, which makes the algorithm more complex. In [14–16], various hybrid algorithms, including the WT, the neutral network and the hidden Markov model, are used to detect the singularity of ECG signals. All of them can complete detecting task precisely but the calculation amount is large, which is not suitable for the application in portable health-care devices. The increase in multiplication operations leads to complexity in computation and application.

In this paper, the existing wavelet transforms in ECG processing are compared carefully. To lower the computational complexity, the Haar function is chosen as the mother wavelet. Based on HWT frequency coefficient, a novel no multiplier structure is proposed. The MMPD is designed to find candidate peak positions of ECG. The Vertex Detection (VD), the Automatic Threshold Correction (ATC) and the execution state machine (ESM) are designed to improve anti-jamming performance. The time shifting in digital processing is eliminated in PPM, which further improves the detection accuracy. The rest of this paper is formed as follows: Section 2 presents the theory of wavelet transform. Section 3 introduces

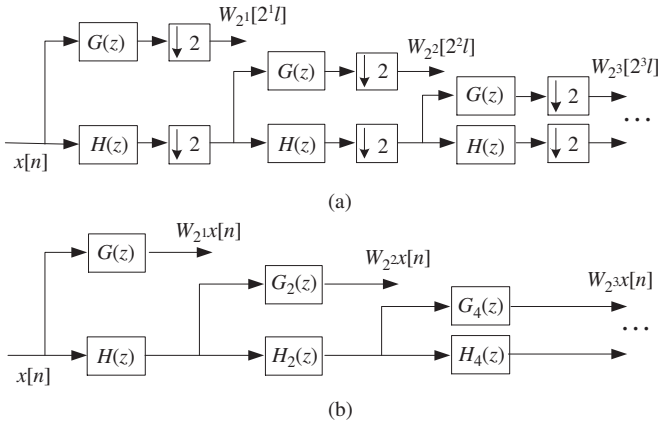

Figure 2 (a) The implementation of DWT with the cascade filter-bank structure; (b) the à trous algorithm without decimation.

the ECG processing method in detail. The computational complexity is analyzed in Section 4. The experimental results and discussion are displayed in Section 5. Finally, the conclusions are made in Section 6.

2 The theory

2.1 The wavelet transform

The wavelet transform is a local transformation on time and scale, which can be applied to extract the feature information of signals. The WT of signal is defined as

$$\mathrm{WT}_x(s,\tau) = f(t) * \psi_s(t) = \frac{1}{\sqrt{s}} \int_{-\infty}^{+\infty} f(t)\psi\left(\frac{t-\tau}{s}\right)\mathrm{d}t, \tag{1}$$

where the $\psi_s(t)$ is the mother wavelet with the scale factor s and the translation τ [17]. When s is index of the power of 2, ($s = 2^j$, j represents integer), it is called dyadic WT. The Mallat algorithm gives the calculation expression of the dyadic WT as follows:

$$W_{2^j} f(n) = \sum_{k\in Z} g_k S_{2^{j-1}} f(n - 2^{j-1}k), \tag{2}$$

$$S_{2^j} f(n) = \sum_{k\in Z} h_k S_{2^{j-1}} f(n - 2^{j-1}k), \tag{3}$$

where $W_{2^j} f(n)$ is the WT of digital signal and S_{2^j} is the smoothing operator. The h_k and g_k are coefficients of a highpass filter and a lowpass filter respectively.

In Figure 2(a), to remove redundant signals, downsamplers are inserted after each filter. At the same time, the temporal resolution is reduced by this way that adds inaccuracies in the estimation of the location of ECG waveform. To obtain smaller translation error, the same sampling rate is employed at all scales. As shown in Figure 2(b), without the downsampling stage, the interpolation arithmetic for the filter frequency response can keep time-invariance and improve the temporal resolution efficiently. In [18], the à trous algorithm is presented, as follow:

$$Q^j(z) = \begin{cases} G(z), & j = 1, \\ G(2z)H(z), & j = 2, \\ G(2^{j-1}z)\prod_{l=0}^{j-2} H(2^l z), & j > 2. \end{cases} \tag{4}$$

Table 1 Comparison of different mother wavelets

Mother wavelet	Scale	The coefficient of frequency response	Taps
Quadratic spline	2^1	$2, -2$	2
	2^2	$0.25, 0.75, 0.5, -0.5, -0.75, -0.25$	6
	2^3	$0.0313, 0.0938, \ldots, -0.0938, -0.0313$	14
	2^4	$0.0039, 0.0017, \ldots, -0.0017, -0.0039$	30
	2^5	$0.00093, 0.00021, \ldots, -0.0021, -0.0093$	62
Haar	2^1	$-0.7071, 0.7071$	2
	2^2	$-0.5, -0.5, 0.5, 0.5$	4
	2^3	$-0.3535, -0.3525, \ldots, 0.3535, 0.3525$	8
	2^4	$-0.25, -0.25, \ldots, 0.25, 0.25$	16
	2^5	$-0.1768, -0.1768, \ldots, 0.1768, 0.1768$	32

2.2 The Haar mother wavelet

In ECG waveform, the P wave, QRS complex and T wave are convex or concave points in time domain, which show different characteristics after WT. The WT has been applied to singularity detection and the performance for ECG signal processing is very good. In addition to accuracy, another important performance of portable health-care devices is the computational complexity. There is no doubt that the amount of calculation in the process of WT is large. Reducing the computational complexity is a main goal in engineering implementation. To accomplish these two seemingly conflicting goals, this paper focuses on the selection of processing tools.

The quadratic spline wavelet transform (QSWT) [19,20] is a popular and widely used tool for ECG signal processing. This algorithm keeps high accuracy and can be implemented with the cascade filter-bank structure. However, the mother wavelet of this method is complex, which will increase the difficulty in implementation.

The HWT is presented and applied to ECG waveform detection in [21]. The Haar function is a set of mutually orthonormal functions, whose support domain is from 0 to 1, and the expression is presented as follows:

$$\psi(t) = \begin{cases} 1, & 0 \leqslant t \leqslant 0.5, \\ -1, & 0.5 < t \leqslant 1. \end{cases} \tag{5}$$

The corresponding filter coefficients are

$$H(\omega) = \frac{1}{\sqrt{2}}(\mathrm{e}^{-\mathrm{j}\omega} + 1), \tag{6}$$

$$G(\omega) = \frac{1}{\sqrt{2}}(\mathrm{e}^{-\mathrm{j}\omega} - 1). \tag{7}$$

Table 1 shows the difference between the quadratic spline mother wavelet and the Haar mother wavelet. Except for the first scale, the QSWT needs more filter taps than the HWT. The absolute value of the HWT frequency response coefficients at one scale is consistent. For the QSWT, the number of coefficients absolute value is $0.5 \cdot$ taps. The number of taps and coefficients at one scale directly determine the computational complexity. The resource and power consumption will increase sharply with the increasing of computational complexity. Therefore, the Haar function is chosen as the mother wavelet for ECG signal processing.

3 The ECG processing method

3.1 The Haar wavelet estimation

In order to test the efficiency of the HWT in ECG signal detection, the HWT of different waveforms at different scales are investigated. As shown in Figure 3, like a and c, the uniphase wave is translated

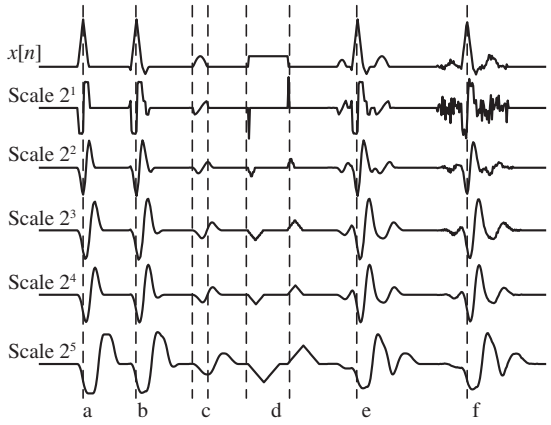

Figure 3 Different waveform and the corresponding HWT coefficients. a, b, c, d, e and f are the HWT of R wave, QRS complex, P or T wave, Rectangular wave, ECG wave and ECG wave with noises respectively.

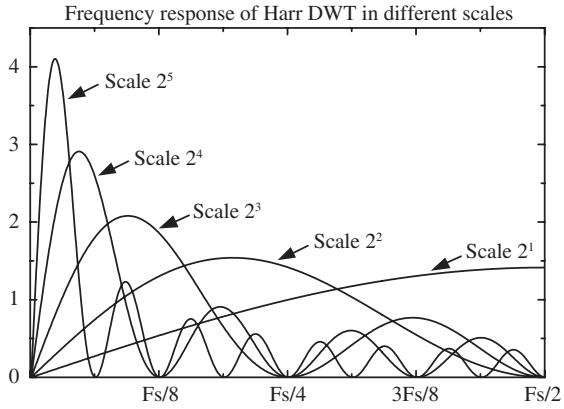

Figure 4 Frequency response of HWT. The Fs is the sampling frequency.

into a negative minimum-positive maximum pair called the modulus maximum pair (MMP). The rising edge and dropping edge match along with the minimum and the maximum respectively. The vertex corresponds to the zero-crossing point between the MMP. This feature can be used to detect the P wave, QRS complex and T wave in ECG waveform. However, there is a delay about $2^{j-1}-1$ [12] between the zero-crossing point and corresponding vertex, and it is a fact that the larger the scale, the greater the deviation. From e and f in Figure 3, it can be seen that the coefficient of scale 2^3 and 2^4 has the better robust performance and the ideal MMP for singularity detection.

The frequency response of HWT is shown in Figure 4, where the range of the window at different scales is determined by the sampling frequency. For ECG signals, the high frequency parts are mainly manifested at small scale and the coefficients at large scale represent the low frequency parts. In [12], it is stated that most energy of ECG is in the low frequency part.

In this paper, the coefficient of HWT at scale 2^4 is selected to delineate the complete ECG waveform. The bandwidth of HWT for the sampling frequency 360/250 at scale 2^4 is mainly at the low frequency part where the energy of ECG is mainly concentrated at. Additionally, the frequency response coefficients at this scale are simple. As shown in Figure 3, the result of transform at scale 2^4 is so clear that it is easy to find the MMP.

However, it is not a single band-pass filter. The HWT is not only to filter out the low and high frequency noises, but also to transform the ECG into the special waveform that is the basis of the waveform detection.

3.2 The HWT

The wavelet transformation is a complex process and occupies the largest part of calculation in ECG processing algorithms. The reason is that a lot of multiplication and addition operations must be executed in the process of WT. The multiplication operations consume large amounts of energy and hardware source. Therefore, reducing the number of multiplication operations is an effective way to reduce the computational complexity for the portable health-care devices.

In Table 1, it shows that the tap coefficients of QSWT are symmetric at every scale. The coefficients of WT are calculated as follow:

$$Y(n) = \sum_{k=1}^{r} a_k * X(n-k). \tag{8}$$

For the portable health-care devices, the calculation amount is large and it's difficult to be implemented.

In this paper, the coefficient at scale 2^4 is chosen to detect the ECG waveform. The calculation

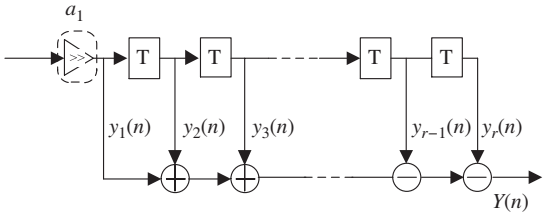

Figure 5 The no multiplier structure of HWT. The $X(n)$ is the input ECG signal. The r reflects the tap of filter. The a reflects the tap coefficient of the equivalent filter. The $y(n)$ is the median value of HWT. $Y(n)$ is the coefficient of HWT. T is the operation cycle.

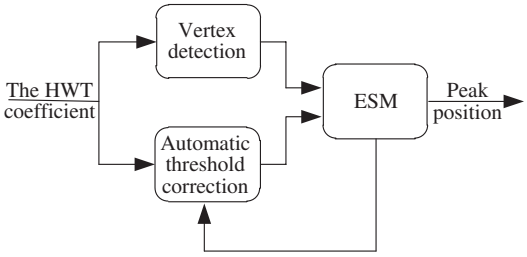

Figure 6 The overall structure of the MMPD.

expression in (8) is modified as follow:

$$y_1(n) = X(n) \gg 2, \tag{9}$$

$$Y(n) = \sum_{k=1}^{r} y_k(n). \tag{10}$$

With (9) and (10), this paper proposes a novel no multiplier structure for HWT, as shown in Figure 5. As the tap coefficient being 1/4, instead of the multiplier, the shift register is applied to get $y_1(n)$. After the input signal $X(n)$ being shifted 2 bit to the right, the computing task of (9) is completed easily and accurately. And then the HWT coefficient $Y(n)$ is obtained by addition and subtraction operations.

For portable health-care devices which monitor ECG signal continuously, the no multiplier structure has less amount of calculation than the traditional one. Additionally, the hardware multipliers consume large amount of area and power in ASIC. The proposed structure is more easily than others', especially for the implementation of ASIC, which is conducive to the miniaturization of portable health-care devices.

3.3 The MMPD

The MMPD which strongly influences the detection accuracy plays an important role in this algorithm. Figure 6 shows the structure of the MMPD, one that consists of three parts, the Vertex Detection (VD), the Automatic Threshold Correction (ATC) and the execution state machine (ESM).

The VD is the pretreatment of the HWT coefficient, which can improve the anti-jamming performance. The processing approach is simple, as shown below:

$$\begin{aligned} &(x[n] < x[n+1])\&(x[n] \leqslant x[n-1]) \Rightarrow \text{Concave Dot},\\ &(x[n] > x[n+1])\&(x[n] \geqslant x[n-1]) \Rightarrow \text{Convex Dot},\\ &\qquad\qquad\qquad\qquad \text{Others} \Rightarrow \text{General Dot}, \end{aligned} \tag{11}$$

$$\left.\begin{array}{l}\text{Concave Dot}\\ \text{Convex Dot}\end{array}\right\} \Rightarrow \text{Vertex}[n] = x[n],$$
$$\text{General Dot} \quad \Rightarrow \text{Vertex}[n] = 0. \tag{12}$$

If $x[n]$ is less or greater than the two adjacent points, $x[n-1]$ and $x[n+1]$, there is a concave point or a convex point and the output Vertex$[n]$ is set to $x[n]$. Otherwise, the Vertex$[n]$ is zero. This approach is designed to remove the interference of non-vertex points with high amplitude. Since the input of ESM is vertex points or zero, the comparison results with the threshold directly determine whether the input points are the modulus maxima points or not.

Through HWT, the peak in time domain is transformed into the MMP. The threshold value classifies the Vertex$[n]$ into two types of points, the modulus maxima points elicited by ECG signals and the general peak points elicited by noises.

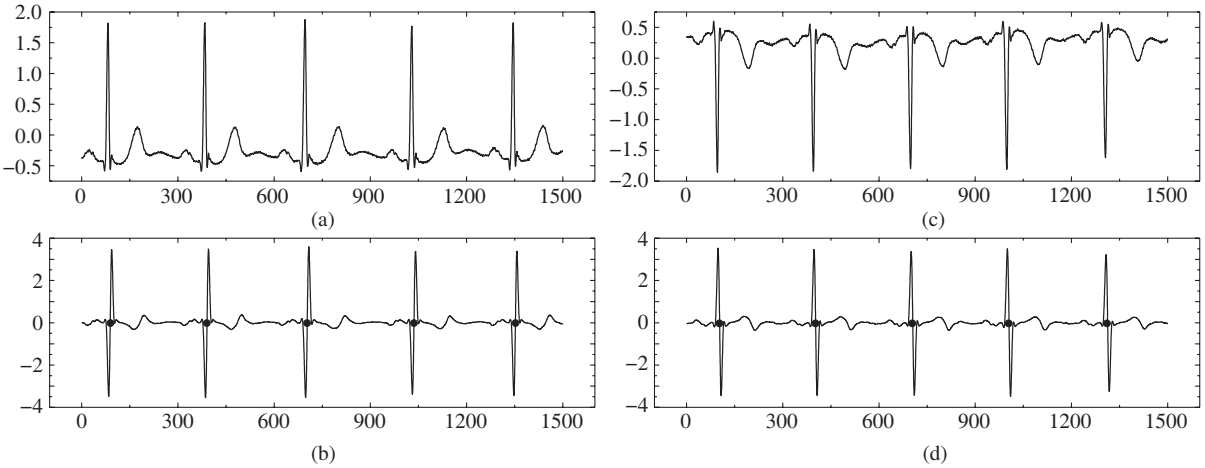

Figure 7 The ECG signal with opposite peaks and the corresponding HWT coefficients. The dots reflect the zero-crossing points between the MMP. (a) ECG signal with positive peaks; (b) HWT coefficient at scale 2^4; (c) ECG signal with negative peaks; (d) HWT coefficient at scale 2^4.

The ATC and the ESM form a feedback network. The ATC provides the decision threshold for the ESM and the ESM passes the peak value to the ATC for updating the threshold. The threshold equation is as follow:

$$\mathrm{TH} = \frac{1}{8}\beta \sum_{n=1}^{8} \mathrm{MM}(n), \tag{13}$$

where TH is the output threshold and the MM(n) is the peak value which is provided by the ESM. The β is the percentage for the average of MM(n). The TH is initialized in the learning stage where 12 pairs of min-max value are chosen and only 8 pairs, which is decided by the MM(n) sorting mechanism, are used to calculate the initial threshold. The MM(n) sorting mechanism is introduced to eliminate the influence of maximum and minimum peak induced by the baseline drift. With (13), two kinds of threshold (positive and negative) can be calculated dynamically.

The ESM is designed to find the MMP, which is used to mark the peak (P wave, QRS complex and T wave) positions in real time. In this part, some decision time is set to improve the anti-interference performance of this algorithm, like the maximum interval (W), which is the time that the QRS complex keeps and the waiting time (F) between adjacent R peaks.

The W is to determine whether there is a MMP. If the interval of the maximum and minimum in one MMP is less than the W, the ESM find a true MMP. Otherwise, the MMP is abandoned. This decision operation is particularly effective to remove the independent modulus maxima interference which may be caused by the baseline drift or other noises.

The F is the free time when there are not the MMP. There aren't any other QRS complex within 200 ms. Therefore, the free time can reduce the rate of false detection. In the free time, the locations of peaks are determined. In this way, the free time is fully used and the peak is positioned without any auxiliary steps.

What's more, there are two kinds of MMPs, one is the negative-positive MMP and the other is the positive-negative one which are the transform wave of the positive peak and the negative peak respectively. In ESM, these two kinds of MMP are distinguished to provide reference for other wave detection.

The MMPD result is shown in Figure 7. As explained in Subsection 3.1, the zero-crossing point within the MMP corresponds to the position of the waveform vertex in time domain. Therefore, for the QRS detection, the dots in Figure 7 are chosen as the candidate position of the R peak.

However, the time shift delay will become larger and larger with the increasing of translation scale. The QRS detection result is shown in Figure 8, where dots are the candidate R peaks. There is obvious disparity between the candidate and the real R peaks, which decreases the detection accuracy. To improve the temporal resolution, the peak position modification (PPM) will be introduced.

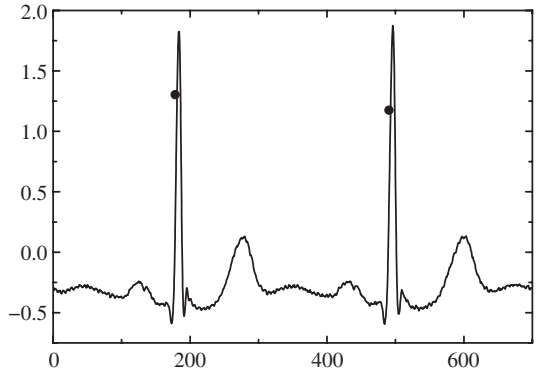

Figure 8 The detection results of R peaks. The dots are the potential R positions found by MMPD.

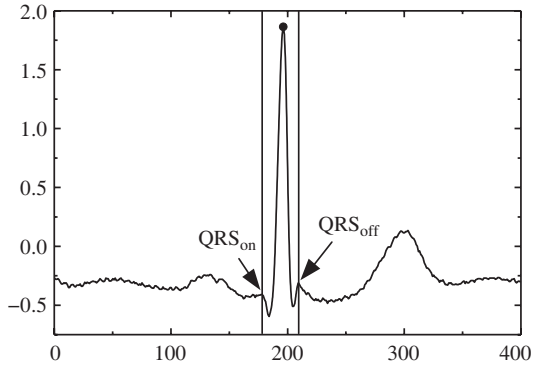

Figure 9 The detection results of QRS complex after the PPM. The dots are R peaks.

3.4 The PPM

The peak position modification (PPM) is to correct the time shift problem in the digital signal processing and determine an accurate position for ECG wave. For example the QRS detection, it first locates the R peak and then accurately finds the Q wave and S wave.

The potential position of R peak is modified at first. The zero-crossing point location t_1 between the MMP is acquired in MMPD. As the analysis in Section 3, there is a delay about $2^{j-1}-1$ between the peak in time domain and the zero-crossing point within the MMP in frequency domain. At the scale 2^4, the delay is about 7 which means the R peak position in time domain is t_1-7 . By simulation, it is found that not all the R peaks are in this position. In order to improve the accuracy, a time window, whose range is from t_1-9 to t_1-1 in time domain, is established. In MMPD, different R peaks (positive or negative) are classified, which provides a great convenience to the PPM. If it is a positive R peak, the location of the maximum value in the time window is chosen as the accurate position of R peak. On the contrary, the location of the minimum value in the time window will be chosen. In this way, the true R peak is located without any deviation.

To describe the whole QRS complex, the onset of QRS ($\mathrm{QRS_{on}}$) and the offset of the QRS ($\mathrm{QRS_{off}}$) must be located at the same time. After the candidate position of R peak being determined in MMPD, the beginning and ending points of the MMP are identified as the candidate points of $\mathrm{QRS_{on}}$ and $\mathrm{QRS_{off}}$ and they are defined as the time t_{on} and t_{off} respectively. Then two time points $\mathrm{QRS_{on}}$ and $\mathrm{QRS_{off}}$ are moved 7 points to the right which means that the $t_{\mathrm{on}}-7$ and the $t_{\mathrm{off}}-7$ are the candidate beginning boundary and the potential ending boundary respectively. Finally the maximum point between $t_{\mathrm{on}}-13$ and $t_{\mathrm{off}}-5$ is determined as the $\mathrm{QRS_{on}}$ point. The $\mathrm{QRS_{off}}$ point can be found in the same way. The detection result is presented in Figure 9, where the locations of R peak, $\mathrm{QRS_{on}}$ and $\mathrm{QRS_{off}}$ are marked clearly.

The width of the time window of PPM in this paper is much narrower than that in [21]. The reason is that the structure in Figure 2(b) is applied. There aren't any down-sampling stages and none of the sampling points are deleted. Therefore, the time-invariance is kept and the temporal resolution is improved greatly.

3.5 The detection of P and T wave

After the outline of QRS complex being delineated, the P and T wave are detected based on the R peak candidate position. Considering the energy of P wave and T wave, which mainly distributes at the scale 2^4 and 2^5 , and the computational complexity, the coefficients of HWT at scale 2^4 are chosen to detect the P and T wave.

In time domain, the P wave is concave or convex which correspond to the MMP in the coefficients of HWT. Because the energy of P wave is less than the QRS complex's, the MMP amplitude for the P wave is much smaller. To solve this problem, a search window that is relative to the R peak potential

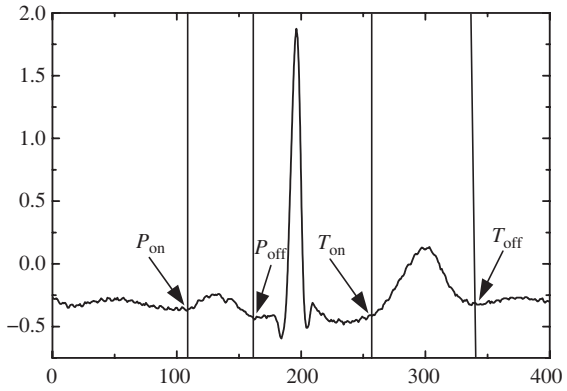

Figure 10 The detection results of P wave and T wave.

1: **initial**
2: input ECG signals $x[n]$
3: **HARR DWT**
4: Calculate the coefficients of the HWT with the no multiplier structure at scale 2^4
5: **Preprocess**
6: The interpolation arithmetic to find the vertices
7: Learning stage to determine the initial decision threshold
8: **QRS detection**
9: find the maximum and the minimum
10: Judge whether it is a true MMP by W
11: The potential positions of QRS_{on}, QRS_{off} and R are t_{on}, t_{off} and t_1 respectively.
12: Determine the R phase
13: **the peak position modification (PPM)**
14: Shift 7 points to left.
15: T1 = t_{on}−7, T2 = t_{off}−7,T3 = t_1−7;
16: if the R phase is positive then
17: find the maximum in the three domain,
QRS_{on}= max [t_{on}−13,t_{on}−5]
QRS_{off}= max [t_{off}−13,t_{off}−5]
R = max [t_1−9,t_1−1]
18: else find the minimum in the three domain,
QRS_{on}= min [t_{on}−13,t_{on}−5]
QRS_{off}= min [t_{off}−13,t_{off}−5]
R= min [t_1−9,t_1−1]
19: end if
20: Update the positive and the negative threshold
21: **P wave detection**
22: Open the window on the left of the R peak
23: Find the MMP
24: find the delineation of the P wave like the QRS detection
25: **T wave detection**
26: find the delineation of the T wave like the P wave detection
27: **Start a new detection cycle**

Figure 11 The flow of this algorithm

position is built. The search window is adjacent to the MMP of the QRS complex, but does not contain it. Obviously, the following process is similar to the step for delineating the boundaries of QRS complex.

The feature of P and T wave is almost the same. Using the algorithm of the P wave detection is easy to describe the outline of T wave. Figure 10 shows the boundary detection results of P and T wave.

4 The computational complexity

The computational complexity will be analyzed in this part. The complexity of subtractions is the same as the additions' and the complexity of comparison is half of the additions, as described in [21]. The result of arithmetic operations is obtained under the condition that the input sample number is N. The flow of this algorithm is shown in Figure 11. The QRS complex, the P and T wave are detected in turn and this algorithm mainly consists of three parts, the HWT, MMPD and PPM.

In HWT stage, this paper proposes a novel no multiplier structure. Compared with the traditional structure, the no multiplier structure is so easy that there are not any multiplication operations. Only $15N$ addition operations are needed to generate the HWT coefficients.

The MMPD stage involves the VD, the ATC and the ESM. The number of comparison operations is N in VD. In ESM, only the nonzero vertex points are compared with the threshold but the number of comparison operations is still considered to be N. The addition operations in ATC are done only when the singularity points (P peak, R peak, and T peak) in ECG signal are detected. The sampling rates of MIT-BIH and QTDB are 360 and 250 respectively. The range of 60–100 is the normal human heart rate. We assume that the heart rate is F and the sampling rate is S. The number of sampling points between

Table 2 The arithmetic operations for different algorithms

Algorithms	Multiplications	Additions
This work	0	$16.33N$
HFEA [21]	$1.093N + 12$ ($N \leqslant 861$)	$2.423N + 214$ ($N \leqslant 861$)
	$1.093N + 10$ ($N > 861$)	$2.553N + 102$ ($N > 862$)

adjacent R peaks can be calculated by $60 \cdot S/F$. Here, the complexity analysis bases on the heart rate 100 and the sampling rate 250, which means that more peaks should be processed, and the number of sampling points between adjacent R peaks is 150 which reveals that there is one R peak in 150 sampling points. The addition operation number for updating one threshold is 7 and one MMP contains two peaks. Finally, the total number of addition operations in ATC for N input sampling is about $0.1N$.

In the PPM stage, for one QRS complex, the number of comparison operations is 24 and the number of addition operations is 6, including three interval ($[t_{\text{on}} - 13, t_{\text{on}} - 5]$ for QRS_{on}, $[t_r - 9, t_r - 1]$ for R_{peak}, $[t_{\text{off}} - 13, t_{\text{off}} - 5]$ for QRS_{off}). Following the principles in ATC complexity analysis, the whole number of comparison and addition operations in this stage is $0.16N$ and $0.04N$ respectively.

The arithmetic operations for P boundaries and T boundaries detection are calculated by the same principle. With the detection being done at the same scale 2^4, there are not any operations in HWT stage. In ATC, the addition operation number is the same as the QRS detection's. Besides, the search window decreases the comparison operations in ESM, only about $N/12$ comparison operations the PPM stage, the operations are the same as the PPM operations for QRS boundaries detection. The total operations are calculated as $0.32N$ comparisons and $0.08N$ additions.

Finally, the total number of all operations for this algorithm is shown in Table 2. Compared with the HFEA, the most superiority of this work is that the detection work is well done without any multiplication operations. Although the number of addition operations is larger than that in HFEA, the analysis principle in this algorithm is more rigorous than that used in HFEA, especially in the PPM stage where the complexity analysis bases on the maximum operating points without any optimization. It's a fact that the power consumption for multiplication operations is much more than that for addition operations. The 0 multiplication operation will decrease the workload and extend the work time under the same battery capacity, which is much attractive for the portable continuous monitoring health-care devices.

In order to estimate the applicability of this algorithm, this algorithm has been coded in Verilog and implemented in the XILINX ML507 development board. Additionally, it has been placed and routed in 0.18 μm CMOS process by the synopsys IC Complier. The overall cell area is only about 0.42 mm^2. As the power consumption being affected by multiple factors, it will be tested after the chip is fabricated in 0.18 μm CMOS process.

5 Validation and discussion

This section is to verify this algorithm with two ECG databases, the MIT-BIH Arrhythmia database (MIT-BIH)[1)] and the QT database (QTDB) [22], and compare with other algorithms to highlight the superiority of this work in the accuracy and computational complexity. In addition, a test system is set up to validate this algorithm further.

5.1 Validation

The MIT-BIH is a set of long-time recordings obtained by the Arrhythmia Laboratory in Beth Israel Hospital. There are 48 records which are over 30 min and selected from 47 subjects. For different records, there are three files, the head, the data and the annotation. In the head files, the sampling rate (360 Hz), the resolution (11-bit) and the voltage range (10 mV) are introduced. The annotation files are to provide annotation information, the heart rhythm and the signal quality, for the data files where ECG

1) MIT-BIH Arrhythmia Database. http://www.physionet.org/physiobank/database/mitdb.

Table 3 The QRS detection results of different algorithms

Reference	Method	FP	FN	Se (%)	Pr (%)
This work	HWT	519	331	99.53	99.70
Ref. [23]	Level-Crossing	1216	651	98.89	99.40
Ref. [24]	Pan-Tompkins			95.65	99.36
Ref. [20]	QSWT	753	330	99.31	99.70
Ref. [19]	QSWT	153	220	99.80	99.86

Table 4 The ECG wave delineation of different algorithms

Reference	Feature	P_{on}	P_{peak}	P_{off}	QRS_{on}	R_{peak}	QRS_{off}	T_{on}	T_{peak}	T_{off}
This work	$\mu\pm\sigma$	4.8±10.1	−4.6±7.3	3.8±13.7	3.6±8.4	−3.9±7.6	5.2±9.3	−4.5±9.9	6.1±16.8	7.8±20.2
Ref. [21]	$\mu\pm\sigma$	−6.3±12.5	5±9.5	3.1±16	3.7±7.8	3.8±9.8	12.1±16.6	−15.8±34 Ref.	15.3±29.3	−16.6±20.8
Ref. [19]	$\mu\pm\sigma$	2.0±14.8	2.0±13.2	1.9±12.8	4.6±7.7		0.8±8.7		0.2±13.9	−1.6±18.1
CSE [25]	2σ	10.2		12.7	6.5		11.6			30.6

signals are stored in the binary format. In fact, the MIH-BIH is one of the most standard databases for validating the QRS detection.

In this paper, all the records are used to examine the accuracy of this algorithm for QRS detection. To evaluate this work, two parameters are defined as Sensitivity (Se) and Positive Prediction (Pr). The equations of Se and Pr are as follow:

$$\text{Se}(\%) = \frac{\text{TP}}{\text{TP} + \text{FN}}, \tag{14}$$

$$\text{Pr}(\%) = \frac{\text{TP}}{\text{TP} + \text{FP}}. \tag{15}$$

The true positive (TP) is the beat that be detected correctly. The false negative (FN) represents the peak number which fails to be detected and the false positive (FP) is the wrong points which are detected as the beat points. The average of Se and Pr is shown in Table 3.

The information of P wave and T wave is not commented in MIT-BIH. The QTDB which presents all kinds of QRS and ST-T morphologies is chosen as the testing source. It is a set of ECG databases whose sources are the MIT-BIH, the European Society of Cardiology ST-T database and some other records from the Beth Israel Deaconess Medical Center. To avoid the baseline shift and other interface, only the signals with low heart rate are selected. This ECG database contains 105 fifteen-min samples with two channel signals from the Holter recording.

In each record, some of ECG signals (between 30 and 100) are annotated by experts. The annotation information consists of the bounds of P, QRS and T wave and the peak positions for P, R and T wave. Because not all the records in QTDB contain the complete annotation information, this paper only chooses these records with complete annotations of the P, QRS and T wave as the testing source. With the help of the manual annotation marked by experts, it is easy for us to classify the ECG waveform into different parts (P_{on}, P_{peak} and P_{off} for P wave, QRS_{on}, R peak and QRS_{off} for QRS complex, T_{on}, T_{peak} and T_{off} for T wave). The test results are shown in Table 4, where μ and σ are the mean and standard deviation respectively.

To fully validate this algorithm, a test system is bulit. The test system contains three parts, the Fluke Medsim 300B patient simulator, the MSP430, and the XILINX ML507 development board. The Fluke Medsim 300B patient simulator is to mimic patient's ECG with different heart rates and phases. The ECG signals are sampled and converted into digital signals by the MSP430. This algorithm has been implemented on the XILINX ML507 development board. The test results are shown in Table 5.

5.2 Discussion

The QRS detection results are shown in Table 3. The performance of WT is much better than that of [23,24]. It is the advantage of WT in ECG signal processing. The accuracy of [19] is slightly better

Table 5 Detection results of the test system

Heart rates	Phase	R Number	Se (%)	Pr (%)
30	positive	3048	100	100
30	negative	3076	100	100
60	positive	3026	100	100
60	negative	3049	100	100
80	positive	3089	100	100
80	negative	3110	100	100
100	positive	3064	100	100
100	negative	3072	100	100

than this work's. However, the Martinez [19] is based on multi-scale transform, which greatly increases the complexity and is not suitable for application. To solve this problem, the Chio-IN [20] and this work detect the ECG signals on one scale transform. Compare with the Chio-IN [20], the test result of this work is better and the complexity is much lower as analyzed in Subsection 2.2. The QRS detection accuracy is an important factor to be considered. Because the QRS contains most of information about cardiac and it's the basis of the complete delineation of ECG waveform. This algorithm can provide more accurate information to users.

In Table 4, the μ and σ represent the difference between test results and the annotations. All ECG boundaries are delineated by this algorithm. Compared with other algorithms, the σ of this work is close to the Martinez's and it is much less than the Mazomenos's. Small σ represents that the detection position is more stable. The CSE is a tolerance standard for the detection of ECG boundaries. Not all the σ in this work satisfies the standard ($\sigma < 2$CSE). In [19,21], however, it is illustrated that the CSE tolerance can not be used to measure all databases because of the annotation difference between databases. Therefore, this algorithm achieves loose criteria in ECG boundaries delineation.

Table 5 shows detection results of the test system. Due to lacking standard annotation information about ECG waveform performed by cardiologists, only the R peak detection accuracy is calculated. In different settings, the Se and Pr are both 100%. This algorithm locates all of the ECG signals accurately, which indicates that it's very suitable for the application in portable health-care devices.

This algorithm achieves high detection accuracy and decreases the computational complexity extremely. They are the key performance to be considered. The detection accuracy of this algorithm is higher than most of ECG processing algorithms, which can help users to improve the diagnostic accuracy. The most advantage of this algorithm is the lowest computational complexity which is analyzed in Section 4. The lower the complexity reduces the difficulty in implementation and application.

The application of this method in portable heath-care devices is alternative, including the software IP and the hardware coprocessor. It can be designed into software IP and embedded into microprocessors. Without occupying any hardware multiplier units, the hardware resource consumed by this algorithm is much less than others', which improves the utilization efficiency of microprocessor greatly. The other option is to implement this algorithm by a hardware coprocessor. As analyzed in this paper, this algorithm is suitable for the ASIC implementation. The ASIC can also be used as the coprocessor of microprocessor. With this coprocessor, multi-process handling can be implemented in portable heath-care devices and more health information can be processed at the same time.

6 Conclusion

In this paper, a low-complexity algorithm with high detection accuracy for ECG signal processing is presented. In order to reduce the computational complexity, the Haar function is chosen as the mother wavelet and only the coefficients at scale 2^4 is applied to detect the ECG waveform. The novel no multiplier structure is proposed to accomplish the wavelet transform. The MMPD with high anti-jamming

finds the MMP for P wave, QRS complex and T wave and provides candidate positions for the corresponding peaks. To solve the time shift problem, the PPM is introduced and it helps improve the detection accuracy. At the same time, with shift and comparison operations, the new method used in PPM lowers the number of comparison operations. Two standard ECG data base, the MIT-BIH Arrhythmia database and the QT database, are applied to verify the accuracy of QRS detection and ECG boundaries detection respectively. The QRS detection result shows high Se (99.53%) and Pr (99.70%). The validation results with QT database are good enough to meet the demand for ECG processing. The computational complexity evaluation for this algorithm is made by calculating the arithmetic operations. About $16.33N$ addition operations and 0 multiplication operations are done when the input sample number is N. Without multiplication operations, the computational complexity is decreased extremely. In application, the structure of the proposed algorithm is suitable for the implementation of ASIC. The proposed low-complexity algorithm is a potential and competitive choice for portable health-care devices, especially the long-time monitoring system.

Acknowledgements

This work was supported by National Basic Research Program of China (973 Program) (Grant No. 2011CB9332-03), National Natural Science Foundation of China (Grant Nos. 61372060, 61076023, 61474107 81300803), National High-tech R&D Program of China (863 Program) (Grants No. 2012AA030308), Grant for Capital Clinical Application Research with Characteristics (Grant No. Z141107002514061).

References

1 Zhang X, Pei W H, Huang B J, et al. A low-noise fully-differential CMOS preamplifier for neural recording applications. Sci China Inf Sci, 2012, 55: 441–452
2 Zhang X, Pei W H, Huang B J, et al. Implantable CMOS neurostimulus chip for visual prosthesis. Sci China Inf Sci, 2011, 54: 898–908
3 Zhang X, Liu M, Wang B, et al. A wide measurement range and fast update rate integrated interface for capacitive sensors array. IEEE Trans Circuits Syst I-Regul Pap, 2014, 61: 2–11
4 Wang Y, Zhang X, Liu M, et al. An implantable sacral nerve root recording and stimulation system for micturition function restoration. IEICE trans Inf Syst, 2014. In press
5 Ye Y L, Sheu P C-Y, Zeng J Z, et al. An efficient semi-blind source extraction algorithm and its applications to biomedical signal extraction. Sci China Ser-F: Inf Sci, 2009, 52: 1863–1874
6 Wang G, Rao N N, Zhang Y, et al. Atrial fibrillatory signal estimation using blind source extraction algorithm based on high-order statistics. Sci China Ser-F: Inf Sci, 2008, 51: 1572–1584
7 An J, Lee J H, Ahn C W. An efficient GP approach to recognizing cognitive tasks from fNIRS neural signals. Sci China Inf Sci, 2013, 56: 109201
8 Kohler B U, Hennig C, Orglmeister R. The principles of software QRS detection. IEEE Eng Med Biol Mag, 2002, 21: 42–57
9 Kleiger R E, Stein P K, Bigger J T. Heart rate variability: measurementand clinical utility. Ann Noninv Electrocardiol, 2005, 10: 88–101
10 Yue Z, Li S X, Li Y, et al. Adaptive R-wave detection method in dynamic ECG with heavy EMG artifact. In: Proceedings of the IEEE International Conference on Information and Automation, Shenyang, 2012. 83–87
11 Hyejung K, Yazicioglu R F, Merken P, et al. ECG signal compression and classification algorithm with quad level vector for ECG holter system. IEEE Trans Inf Technol Biomed, 2010, 14: 93–100
12 Li C W, Zheng C X, Tai C F. Detection of ECG characteristic points using wavelet transforms. IEEE Trans Biomed Eng, 1995, 42: 21–28
13 Zhang F, Lian Y. QRS detection based on multiscale mathematical morphology for wearable ECG devices in body area networks. IEEE Trans Biomed Circuits Syst, 2009, 3: 220–228
14 Dokur Z, Olmez T, Yazgan E. ECG waveform classification using the neural network and wavelet transform. In: Proceedings of the IEEE International Conference on Medicine and Biology, Atlanta, 1999. 273–273
15 Szilágyi S, Szilágyi L. Wavelet transform and neural-network basedadaptive filtering for QRS detection. In: Proceedings of the IEEE International Conference on Medicine and Biology, Chicago, 2000. 1267–1270
16 Andre R V A, Boudy J. Combining wavelet transform and hidden Markov models for ECG segmentation. EURASIP J Appl Signal Process, 2007, 2007: 056215
17 Mallat S. A Wavelet Tour of Signal Processing. New York: Academic, 2009. 102–115

18 Cohen A, Kovačević J. Wavelets: the mathematical background. Proc IEEE, 1996, 84: 514–522
19 Martinez J P, Almeida R, Olmos S, et al. A wavelet-based ECG delineator: evaluation on standard databases. IEEE Trans Biomed Eng, 2004, 51: 570–581
20 Chio-In I, Pui-In M, Chi-Pang L, et al. A 0.83-μW QRS detection processor using quadratic spline wavelet transform for wireless ECG acquisition in 0.35-μm CMOS. IEEE Trans Biomed Circuits Syst, 2012, 6: 586–595
21 Mazomenos E B, Biswas D, Acharyya A, et al. A low-complexity ECG feature extraction algorithm for mobile healthcare applications. IEEE J Biomed Health Inf, 2013, 17: 459–469
22 Laguna P, Mark R G, Goldberg A, et al. A database for evaluation of algorithms for measurement of QT and other waveform intervals in the ECG. In: Proceedings of the IEEE International Conference in Computers on Cardiology, Lund, 1997. 673–676
23 Ravanshad N, Rezaee-Dehsorkh H, Lotfi R, et al. A level-crossing-based QRS-detection algorithm for wearable ECG sensors. IEEE J Biomed Health Inf, 2013, 18: 183–192
24 Wang H M, Lai Y L, Hou M C, et al. A 6 ms-accuracy, 0.68 mm^2 and 2.21 μW QRS detection ASIC. In: Proceedings of the IEEE International Conference on Circuits and Systems, Pairs, 2010. 1372–1375
25 Willems J L. Recomendations for measurement standards in quantitative electrocardiography. Eur Heart J, 1985, 6: 815–825